Inorganic Chemistry

Article

pubs.acs.org/IC

Oxothiomolybdenum Derivatives of the Superlacunary Crown Heteropolyanion $\{P_8W_{48}\}$: Structure of $[K_4\{Mo_4O_4S_4(H_2O)_3(OH)_2\}_2(WO_2)(P_8W_{48}O_{184})]^{30-}$ and Studies in Solution

Vladimir S. Korenev,[†,‡] Sébastien Floquet,*[,†] Jérôme Marrot,[†] Mohamed Haouas,[†] Israël-Martyr Mbomekallé,[†] Francis Taulelle,[†] Maxim N. Sokolov,[‡] Vladimir P. Fedin,[‡] and Emmanuel Cadot*[,†]

[†]Institut Lavoisier de Versailles, UMR 8180, University of Versailles, 45 avenue des Etats-Unis, 78035 Versailles, France

[‡]Nikolaev Institute of Inorganic Chemistry, Siberian Branch of the Russian Academy of Science, Novosibirsk 630090, Russia

Supporting Information

ABSTRACT: Reaction of the cyclic lacunary $[H_7P_8W_{48}O_{184}]^{33-}$ anion (noted P_8W_{48}) with the $[Mo_2S_2O_2(H_2O)_6]^{2+}$ oxothiocation led to two compounds, namely, $[K_4\{Mo_4O_4S_4(H_2O)_3(OH)_2\}_2(WO_2)(P_8W_{48}O_{184})]^{30-}$ (denoted **1**) and $[\{Mo_4O_4S_4(H_2O)_3(OH)_2\}_2(P_8W_{48}O_{184})]^{36-}$ (denoted **2**), which were characterized in the solid state and solution. In the solid state, the structure of $[K_4\{Mo_4O_4S_4(H_2O)_3(OH)_2\}_2(WO_2)(P_8W_{48}O_{184})]^{30-}$ reveals the presence of two disordered $\{Mo_4O_4S_4(H_2O)_3(OH)_2\}^{2+}$ "handles" connected on both sides of the P_8W_{48} ring. Such a disorder is consistent with the presence of two geometrical isomers where the relative disposition of the two $\{Mo_4O_4S_4(H_2O)_3(OH)_2\}^{2+}$ handles are arranged in a perpendicular or parallel mode. Such an interpretation is fully supported by ^{31}P and ^{183}W NMR solution studies. The relative stability of both geometrical isomers appears to be dependent upon the nature of the internal alkali cations, i.e., Na^+ vs K^+, and increased lability of the two $\{Mo_4O_4S_4(H_2O)_3(OH)_2\}^{2+}$ handles, compared to the oxo analogous, was clearly identified by significant broadening of the ^{31}P and ^{183}W NMR lines. Solution studies carried out by UV−vis spectroscopy showed that formation of the adduct $[\{Mo_4O_4S_4(H_2O)_3(OH)_2\}_2(P_8W_{48}O_{184})]^{36-}$ occurs in the 1.5−4.7 pH range and corresponds to a fast and quantitative condensation process. Furthermore, ^{31}P NMR titrations in solution reveal formation of the "monohandle" derivative $[\{Mo_4O_4S_4(H_2O)_3(OH)_2\}(P_8W_{48}O_{184})]^{38-}$ as an intermediate prior to formation of the "bishandle" derivatives. Furthermore, the electrochemical behavior of $[\{Mo_4O_4S_4(H_2O)_3(OH)_2\}_2(P_8W_{48}O_{184})]^{36-}$ was studied in aqueous medium and compared with the parent anion P_8W_{48}.

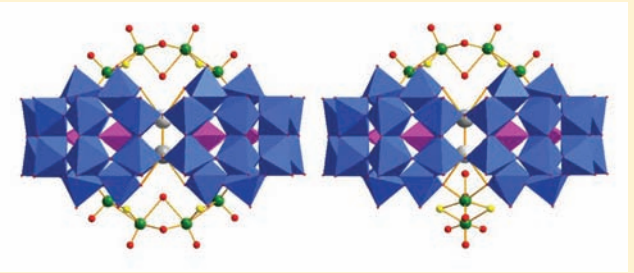

INTRODUCTION

Current development in the chemistry of polyoxometalates (POMs) is widely driven by potential applications in catalysis,[1] medicine,[2] magnetism,[3,4] materials sciences, and nanotechnology.[5−8] Accumulation of transition metal centers in a single nanoscopic inorganic cluster can play a crucial role for catalytic and electrocatalytic properties. Selective condensation of cationic metallocomplex units on nucleophilic lacunary precursors corresponds to a useful approach to synthezise high-nuclearity POMs. In such a context, vacant polyoxotungstates constitute ideal candidates because they exhibit remarkable rigidity and robustness. In this field, the cyclic superlacunary anionic POM $[H_7P_8W_{48}O_{184}]^{33-}$ (P_8W_{48}) isolated in 1985 by Contant and Tezé[9] represents an attractive system which exhibits a high propensity to include various metallic cations in its large anionic pocket. Actually, the host−guest chemistry based on the superlacunary P_8W_{48} was investigated and widely demonstrated through structural characterization of a large series of complexes including various metallic cations such as copper,[10−17] iron,[18] cobalt,[19,20] nickel,[20] manganese,[20−22] or lanthanides,[23] organometallic moieties such as [Ru(p-cymene)],[24,25] and even oxometallic clusters.[20,26,27]

In this way, combinations with the dinuclear oxothiocation $[Mo_2O_2S_2]^{2+}$ with P_8W_{48} should be promising to give new insights about the coordination/condensation properties of this large macrocyclic ion. P_8W_{48} represents a stable and an electroactive component which could be viewed as an electron storage unit,[16−18,28] while the $\{Mo_2O_2S_2\}$-based materials are able to promote electrocatalysis, such as proton reduction into hydrogen.[29−31] Thus, some synergistic effects could be expected from combinations of both components within a single complex unit.

The dinuclear cation $[Mo_2O_2S_2(H_2O)_6]^{2+}$ exhibits coordination requirements restricted to three available sites on each molybdenum center, thus allowing one to develop predictable POM−$\{Mo_2O_2S_2\}$ based coordination chemistry. The oxothiocation has been proved to react with basic lacunary POMs such as PW_9,[32] AsW_9,[33] SiW_{10},[34] PW_{10},[35] PW_{11},[36] P_2W_{15},[37] and

Received: October 30, 2011
Published: January 23, 2012

   dx.doi.org/10.1021/ic202346r | *Inorg. Chem.* 2012, 51, 2349−2358

P_2W_{17}[38] to give species ranging from monomeric to tetramodular assembly.

Herein we report on the synthesis and characterization of combinations between the P_8W_{48} and the $[Mo_2O_2S_2]^{2+}$ moieties. The synthesis and structure of the addition compounds based on the $[\{Mo_4O_4S_4(H_2O)_3(OH)_2\}_2(P_8W_{48}O_{184})]^{36-}$ architecture are described and discussed. Particular attention is focused on the study of the association process in solution, which highlights formation of an intermediate species $[\{Mo_4O_4S_4(OH)_2(H_2O)_3\}P_8W_{48}]^{38-}$ prior to formation of two saturated geometric isomers, denoted *para* and *perp*. Furthermore, electrochemical data of the $\{Mo_2O_2S_2\}$-containing P_8W_{48} compound are also given.

EXPERIMENTAL SECTION

Physical Methods. Water content was determined by thermal gravimetric analysis (tga7, Perkin-Elmer). Infrared spectra were recorded on a Magna 550 Nicolet spectrophotometer in KBr pellets. Elemental analyses were performed by the Service central d'analyze du CNRS, Vernaison, France and by the Service d'analyze du CNRS, ICSN, Gif sur Yvette, France. Energy-dispersive X-ray spectroscopy (EDX) measurements were performed on a JEOL JSM 5800LV apparatus.

Spectrophotometric studies were carried out on a Perkin-Elmer Lambda 19 spectrophotometer. Stability studies were carried out with 0.1 mM solutions of the relevant polyanion. Matched 1 cm optical path length quartz cuvettes were used. The compositions of the various media were as follows: for pH 1, 2, and 3 0.5 M Li_2SO_4 + H_2SO_4; for pH 4 and 5 1.0 M CH_3COOLi + CH_3COOH. Spectrophotometric titrations were performed at room temperature in quartz cells of 1 mm path length. Stock solutions (2.25×10^{-3} M) of P_8W_{48} in 1 M LiCl at pH = 1.5, 3, or 4.7 and 2.25×10^{-3} M stock solutions of $[Mo_2O_2S_2]^{2+}$ (4.5×10^{-4} M of $K_{2-x}(NMe_4)_x[I_2Mo_{10}O_{10}S_{10}(OH)_{10}(H_2O)_5]\cdot 20H_2O$ (with x between 0 and 0.5) in 1 M LiCl at pH = 1.5, 3, or 4.7 were prepared by dissolution of P_8W_{48} or $K_{2-x}(NMe_4)_x[I_2Mo_{10}O_{10}S_{10}(OH)_{10}(H_2O)_5]\cdot 20H_2O$ in 1 M LiCl followed by adjustment of the pH, 1.5 and 3, with HCl. The batch method was used to prepare samples with ratios $[Mo_2O_2S_2]^{2+}/P_8W_{48}$ ranging from 0 to 4 in 1 M LiCl at pH = 1.5 and 3. The concentrations of the $[Mo_2O_2S_2]^{2+}$ chromophore were maintained constant by adjusting the total volumes with 1 M LiCl adjusted at pH = 1.5 or 3. The samples were left to equilibrate overnight at room temperature before taking readings. A similar procedure was followed for pH = 4.7 except that the solutions were prepared in CH_3COOH/CH_3COOLi buffer (1M/1M).

NMR Measurements. Solution ^{31}P NMR measurements were performed on a Bruker Avance 300 instrument operating at 121.5 MHz in 5 mm o.d. tubes. Chemical shifts were referenced to 85% H_3PO_4 solution. ^{31}P NMR titrations were performed at pH = 1, 2, and 3 as follows: a 4.5×10^{-3} M stock solution of P_8W_{48} in 1 M LiCl at pH = 1, 2, or 3 was obtained by dissolving solid P_8W_{48} in 1 M LiCl and adjusting the required pH with HCl. To increase the solubility, the major part of the potassium countercations associated to P_8W_{48} were replaced by sodium through addition of $NaBPh_4$ (24 equiv per P_8W_{48} units) and removing the resulting white precipitate of $KBPh_4$. Alternatively, 4.5×10^{-2} M stock solutions of $[Mo_2O_2S_2]^{2+}$ in 1 M LiCl at pH = 1, 2, or 3 were prepared without addition of $NaBPh_4$ as described above. Samples with ratios $[Mo_2O_2S_2]^{2+}/P_8W_{48}$ ranging from 0 to 4 were prepared by mixing required amounts of $Mo_2O_2S_2$ solutions (0–0.4 mL) with 1 mL of the P_8W_{48} stock solution under stirring followed by addition of 0.1 mL of D_2O. The samples were left to equilibrate under stirring overnight at room temperature. Solid-state ^{31}P NMR spectra were measured at room temperature under magic angle spinning (MAS) condition. NMR spectra were obtained on a Bruker Avance-500 spectrometer equipped with a MAS accessory operating at 202.456 MHz. A zirconium oxide cylindrical-type rotor was used. Spectra were recorded with a single 45° pulse (2.4 μs) at a spinning rate of about 30 kHz (no spinning side bands were observed). The spectral width and data points were 15 kHz and 2 k, respectively. Spectra with reasonable signal-to-noise ratios were obtained after 48 transients at a repetition time of 80 s. Chemical shifts were calibrated relative to $(NH_4)H_2PO_4$ as an external standard (set to δ = 0 ppm). The experimental errors of the ^{31}P chemical shifts were estimated to be ±0.4 ppm. Solution ^{183}W NMR (20.833 MHz) spectra were recorded at 26 °C in 10 mm o.d. tubes on a Bruker Avance-500 FT-NMR spectrometer equipped with a Bruker BBO low-frequency tunable probe and Bruker Topspin data-acquisition software. These spectra were calibrated to an external secondary reference of SiW_{12}–D_2O solution (δ = −103.8 ppm). The peaks were decomposed by least-squares computer fitting assuming pure Lorentzian shape for the solution spectra and combined Gaussian and Lorentzian broadening function for solid spectra; the chemical shift, half width, and intensity of each peak were then estimated. The composite curves reproduced well the experimental spectra.

Electrochemistry Studies. Purified water was used throughout. It was obtained by passing water through a RiOs 8 unit followed by a Millipore-Q Academic purification set. All reagents were of high-purity grade and used as purchased without further purification. The compositions of the various media were as follows: for pH 1, 2, and 3 0.5 M Li_2SO_4 + H_2SO_4; for pH 4 and 5 1.0 M CH_3COOLi + CH_3COOH. The polyanion concentration was 0.2 mM. All cyclic voltammograms were recorded at 10 mV s^{-1} scan rate unless otherwise stated. Solutions were deaerated thoroughly for at least 30 min with pure argon and kept under a positive pressure of this gas during the experiments. The source, mounting, and polishing of the glassy carbon (GC, Carbone Lorraine, France) electrodes have been described.[39] The glassy carbon samples had a diameter of 3 mm. Controlled potential coulometry experiments were performed with a large surface area glassy carbon plate as the working electrode. The auxiliary electrode was a Pt plate placed within a fritted-glass isolation chamber. Potentials are quoted against a saturated calomel electrode (SCE). The electrochemical setup was an EG&G 273 A potentiostat controlled by a PC with the M270 software. All experiments were performed at room temperature.

X-ray Diffraction Studies. The structure of **KLi-1** was obtained from single crystals of $K_{20}Li_6H_4[K_4\{Mo_4O_4S_4(H_2O)_3(OH)_2\}_2(WO_2)(P_8W_{48}O_{184})]\cdot 95H_2O$. A parallelepipedic red single crystal was mounted in a capillary. Dimensions of the crystal and cell parameters are given in Table 1. X-ray intensity data were collected at 293 K on a Bruker-Nonius X8-APEX2 CCD area detector diffractometer using Mo Kα radiation (λ = 0.71073 Å). Data reduction was accomplished using SAINT V7.03 (APEX2 version 1.0-8; Bruker AXS: Madison, WI, 2003). The substantial redundancy in data allowed a semiempirical absorption correction (SADABS V2.10) to be applied on the basis of multiple measurements of equivalent reflections. The structure was solved by direct methods, developed by successive difference Fourier syntheses, and refined by full-matrix least-squares on all F^2 data using SHELXTL V6.12 (SHELXTL version 6.12; Bruker AXS: Madison, WI, 2001). Heavy atoms were initially located by direct methods. The remaining non-hydrogen atoms were located from Fourier differences and refined with anisotropic thermal parameters. All atoms were anisotropically refined except for some disordered free water molecules. Figures 1–4 were generated by Diamond version 3.2g (copyright Crystal Impact GbR). The crystal structure may be obtained from the Fachinformationszentrum Karlsruhe, 76344, Eggenstein-Leopoldshafen, Germany (crystaldata@fiz-karlsruhe.de) on quoting depository number 423504.

Syntheses. Precursors $K_{2-x}(NMe_4)_x[I_2Mo_{10}O_{10}S_{10}(OH)_{10}(H_2O)_5]\cdot 20H_2O$ (x < 0.5) and $K_{28}Li_5H_7[P_8W_{48}O_{184}]\cdot 92H_2O$ (P_8W_{48}) were prepared as described in the literature and characterized by routine methods (FT-IR, NMR, EDX, TGA).[9,40] More details on the NMR data are given in Tables 2 and 3.

$K_{20}Li_6H_4[K_4\{Mo_4O_4S_4(OH)_2(H_2O)_3\}_2(WO_2)(P_8W_{48}O_{184})]\cdot 95H_2O$, KLi-1. P_8W_{48} (1 g, 0.068 mmol) and LiCl (0.5 g, 11.765 mmol) were dissolved in 25 mL of H_2O. The pH was adjusted to 2 with a few drops of 6 M HCl. The solution was heated to 55–60 °C, and $K_{2-x}(NMe_4)_x[I_2Mo_{10}O_{10}S_{10}(OH)_{10}(H_2O)_5]\cdot 20H_2O$ (0.128 g, 0.056 mmol) was added. The solution color changed from colorless to red. The mixture was heated at 55–60 °C about 4 h. The resulting solution was covered with Parafilm, and crystals were obtained within a few days.

dx.doi.org/10.1021/ic202346r | Inorg. Chem. 2012, 51, 2349–2358

Table 1. Relevant Crystallographic Data for 1

	1
formula	$H_{210}K_{24}Li_6Mo_8O_{299}P_8S_8W_{49}$
M, g·mol^{-1}	16 256.13
T, K	293(2)
wavelength/Å	0.71073
cryst size (mm)	0.16 × 0.10 × 0.06
cryst syst	tetragonal
space group	$I4/mmm$
a, Å	26.7803(11)
b, Å	26.7803(11)
c, Å	21.4115(10)
α, deg	90
β, deg	90
γ, deg	90
V, Å^3	15356.0(11)
Z	2
D_{calcd}/g cm^{-3}	3.516
μ/mm^{-1}	19.120
θ range for data collection	1.08−30°
F(000)	13 128
completeness to θ_{max}/%	99.9
limiting indices	$-37 \le h \le 37$
	$-33 \le k \le 37$
	$-30 \le l \le 28$
data/restraints/params	6135/0/261
R(int)	0.0619
goodness-of-fit on F^2	1.191
final R indices [$I > 2\sigma(I)$]	R1[a] = 0.0684
	wR2[b] = 0.1849
largest diff. peak and hole/e·A^{-3}	4.000 and −6.409

[a] $R1 = (\sum||F_o| - |F_c||)/(\sum|F_c|)$. [b] $Rw = ((\sum w(F_o^2 - F_c^2)^2)/(\sum w(F_o^2)^2))^{1/2}$, $1/w = \sigma^2F_o^2 + (aP)^2 + bP$.

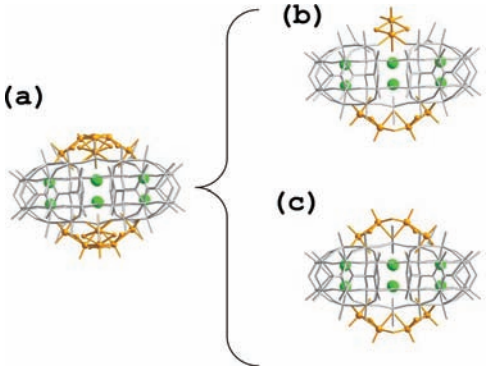

Figure 1. (a) Representation of the structural disorder involving two $\{Mo_4S_4(OH)_2(OH_2)_3\}^{2+}$ grafted on both sides of the $\{P_8W_{48}\}$ surface as the superimposition of two geometrical isomers with perpendicular (b) and parallel disposition (c). Color code: gray sticks = P_8W_{48} framework; orange sticks = $\{Mo_4S_4(OH)_2(OH_2)_3\}$ basket handle; green spheres = disordered potassium cations.

Yield: ca. 0.6 g of red crystals (54%). IR/cm^{-1} (KBr pellet): 1138(m), 1080(m), 1013(w), 956(m), 932(s), 910(s), 817(s, br), 747(s, br), 709(s, br), 666(sh), 571(m), 517(m), 459(w). TGA: An average loss of ca. 100 water molecules between room temperature and 200 °C corresponding to crystallization and coordinated water molecules. Anal. Calcd for $K_{20}Li_6H_4[K_4\{Mo_4O_4S_4(OH)_2(H_2O)_3\}_2(WO_2)(P_8W_{48}O_{184})]\cdot 95H_2O$ (M = 16 256.1 g mol^{-1}): K, 5.77; Li, 0.26; P, 1.52; Mo, 4.72; W, 55.41; H, 1.30; S, 1.58. Found: K, 5.49; Li, 0.23; P, 1.60; Mo, 4.76; W, 54.26; H, 1.10; S, 1.82. EDX atomic ratios

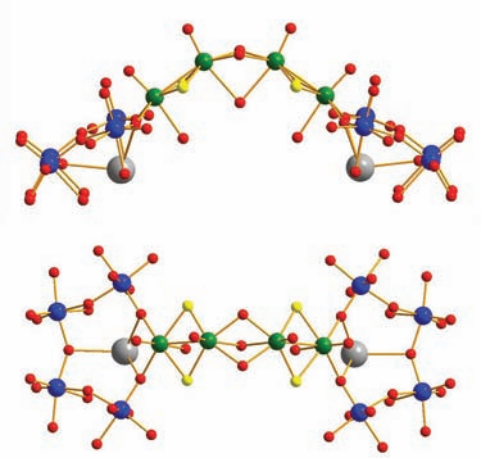

Figure 2. Top and side views of the coordination of the $[Mo_4O_4S_4(OH)_2(H_2O)_3]^{2+}$ handles and the potassium cations with the $\{P_8W_{48}\}$ moiety.

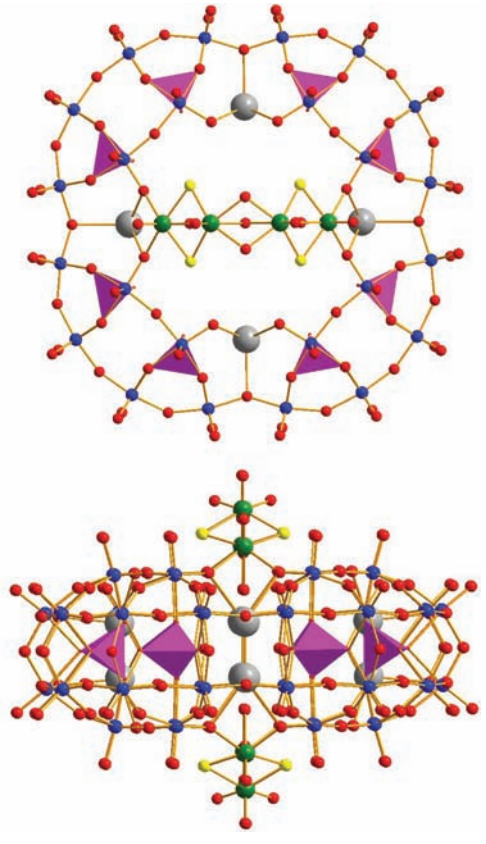

Figure 3. Top and side views of the parallel isomer *para*-$[K_4P_8W_{48}O_{184}(Mo_4O_4S_4(OH)_2(H_2O)_3)_2]^{32-}$ of **1** in ball-and-stick representation. Additional disordered tungstate groups are ommited. Phosphates are depicted in pink polyhedra, tungsten in blue, molybdenum in green, potassium in gray, oxygen in red, and sulfur in yellow.

calculated for $K_{20}Li_6H_4[K_4\{Mo_4O_4S_4(OH)_2(H_2O)_3\}_2(WO_2)(P_8W_{48}O_{184})]\cdot 95H_2O$ (found): W/Mo = 6.12 (6.31); Mo/S = 1.00 (1.12); W/K = 2.04 (2.03); W/P = 6.12 (6.38).

$K_{26}Li_2H_8[\{Mo_4O_4S_4(OH)_2(H_2O)_3\}_2(P_8W_{48}O_{184})]\cdot 90H_2O$, KLi-2. P_8W_{48} (3 g, 0.203 mmol) and LiCl (3.4 g, 80 mmol) were dissolved in 80 mL of 0.1 M HCl. $NaBPh_4$ (1.6 g, 4.678 mmol, ~23 equiv) was added to remove potassium cations as a white precipitate $KBPh_4$. $K_{2-x}(NMe_4)_x[I_2Mo_{10}O_{10}S_{10}(OH)_{10}(H_2O)_5]\cdot 20H_2O$ (0.385 g, 0.167 mmol)

dx.doi.org/10.1021/ic202346r | Inorg. Chem. 2012, 51, 2349−2358

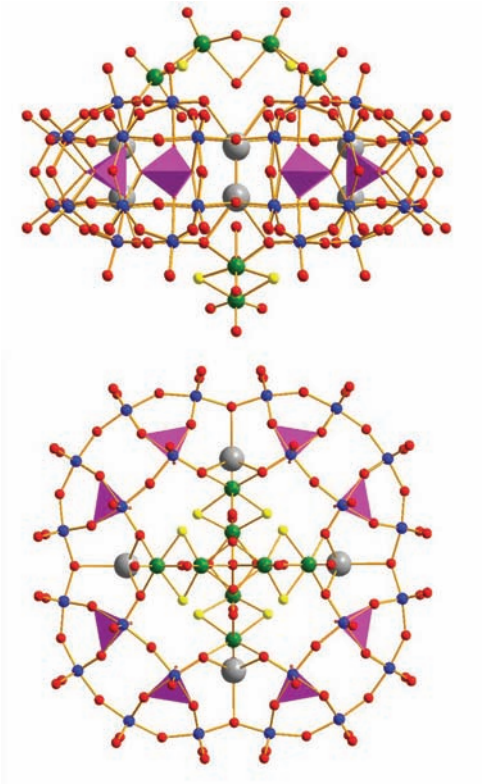

Figure 4. Top and side views of the perpendicular isomer *perp*-$[K_4P_8W_{48}O_{184}(Mo_4O_4S_4(OH)_2(H_2O)_3)_2]^{32-}$ in **1** in ball-and-stick representation. Additional disordered tungstate groups are ommited. Phosphates are depicted in pink polyhedra, tungsten in blue, molybdenum in green, potassium in gray, oxygen in red, and sulfur in yellow.

Table 2. ^{31}P NMR Data in LiCl (1 M)

compounds	signals/relative integration/bandwidth
P_8W_{48}	−6.56 ppm/1/3 Hz
KLi-2	−7.54 ppm/0.26/3 Hz
	−8.18 ppm/0.53/3 Hz
	−8.92 ppm/0.21/12 Hz
NaK-2	−7.31 ppm/0.37/3 Hz
	−8.35 ppm/0.30/56 Hz
	−9.42 ppm/0.33/12 Hz
NaK-2 + 5 equiv of KCl	−7.31 ppm/0.37/3 Hz
	−7.92 ppm/0.30/14 Hz
	−9.02 ppm/0.33/21 Hz
NaK-2 + 10 equiv of KCl	−7.31 ppm/0.37/3 Hz
	−7.95 ppm/0.30/10 Hz
	−8.97 ppm/0.33/23 Hz
Na-2	−7.36 ppm/ca. 0.06/35 Hz
	−8.15 ppm/0.90/55 Hz
	−9.29 ppm/ca. 0.04/60 Hz
Na-2 + 10 equiv of KCl	−7.29 ppm/ca. 0.06/16 Hz
	−7.86 ppm/0.90/12 Hz
	ca. −8.95 ppm, very broad

was added, provoking color change from colorless to dark red. The limpid mixture was stirred at room temperature. After 6 h, KCl (2 g, 26.846 mmol) was added to give a red-orange precipitate, which was collected by filtration, washed with water, ethanol, and ether, and dried in air. Yield: ca. 2.2 g of crude potassium salt (66%). ^{31}P NMR in aqueous molar LiCl/ppm: −7.54, −8.18, −8.92. IR/cm^{-1} (KBr pellet): 1140(m), 1081(m), 1015(w), 956(m), 933(s), 912(s), 819(s, br), 758(s, br), 712(s, br), 668(sh), 569(m), 517(m), 458(w). TGA: Loss of ca. 95 water molecules between room temperature and 200 °C corresponding to free and coordinated water molecules. Anal. Calcd for $K_{26}Li_2H_8[\{Mo_4O_4S_4(OH)_2(H_2O)_3\}_2(P_8W_{48}O_{184})]\cdot 90H_2O$ (M = 16004.1 g mol^{-1}): K, 6.35; Li, 0.09; P, 1.55; Mo, 4.80; W, 55.14; H, 1.28; S 1.60. Found: K, 6.16; Li, 0.08; P, 1.64; Mo, 4.95; W, 53.93; H, 0.98; S, 1.79. EDX atomic ratio calculated for $K_{26}Li_2H_8[\{Mo_4O_4S_4(OH)_2(H_2O)_3\}_2(P_8W_{48}O_{184})]\cdot 90H_2O$ (found): W/Mo = 6.0 (6.03); Mo/S = 1 (0.96); W/K = 1.85 (1.73); W/P = 6.0 (6.25).

$Na_{25}K_2LiH_8[\{Mo_4O_4S_4(OH)_2(H_2O)_3\}_2(P_8W_{48}O_{184})]\cdot 125H_2O$, NaK-2. The beginning of the procedure is similar to that described above for compound **KLi-2**. The red resulting solution was stirred for 5 h; then NaCl (10 g, 171 mmol) was added to give a red crystalline precipitate. After 12 h at 4−6 °C, crystalline material was collected by filtration, washed with water, ethanol, and ether, and dried in air. Yield: ca. 0.755 g of the crystalline mixed Na/K/Li salt denoted **NaK-2** (yield 23%). ^{31}P NMR in aqueous molar LiCl/ppm: −7.31, −8.35, −9.42. IR/cm^{-1} (KBr pellet): 1140(m), 1083(m), 1020(w), 961(s), 939(s), 915(s), 841(sh, br), 780(s, br), 714 (s, br), 661(sh, br), 570(m), 512(m), 462(w). TGA: Loss of ca. 130 water molecules between room temperature and 200 °C corresponding to free and coordinated water molecules. Anal. Calcd for $Na_{25}K_2LiH_8[\{Mo_4O_4S_4(OH)_2(H_2O)_3\}_2(P_8W_{48}O_{184})]\cdot 125H_2O$ (M = 16264.1 g mol^{-1}): Na, 3.53; K, 0.48; Li, 0.04; P, 1.52; Mo, 4.72; W, 54.26; H, 1.70; S, 1.58. Found: Na, 3.27; K, 0.45; Li, 0.04; P, 1.35; Mo, 4.19; W, 54.00; H, 1.35; S, 1.60. EDX atomic ratio calculated for $Na_{25}K_2LiH_8[\{Mo_4O_4S_4(OH)_2(H_2O)_3\}_2(P_8W_{48}O_{184})]\cdot 125H_2O$ (found): W/Mo = 6.00 (6.10); Mo/S = 1.00 (1.03); W/P = 6.00 (6.13); W/Na = 1.92 (2.08); W/K = 12.0 (11.18).

$Na_{28}H_8[\{Mo_4O_4S_4(OH)_2(H_2O)_3\}_2(P_8W_{48}O_{184})]\cdot 130H_2O\cdot\sim 8$ NaCl, Na-2. The beginning of the procedure is similar to that described above for the previous compound. The dark red-colored filtrate collected after precipitation of **NaK-2** was allowed to stand for crystallization in air. After several days, red crystalline compound mixed with colorless crystals of NaCl was obtained. The red crystals denoted **Na-2** were separated mechanically from NaCl, washed with ethanol and ether, and dried in air. Yield: 0.67 g (~21%). ^{31}P NMR in aqueous molar LiCl/ppm: −7.36, −8.15, −9.29 (very broad). IR/cm^{-1} (KBr pellet): 1141(m), 1084(m), 1020(w), 961(s), 937(s), 915(s), 828(sh, br), 770(s, br), 713(s, br), 668(sh, br), 571(m), 523(m), 461(w). TGA: Loss of ca. 135 water molecules between room temperature and 200 °C corresponding to free and coordinated water molecules.

Table 3. ^{183}W NMR Data in LiCl (1 M) Compared to Literature Data

compounds	chemical shifts, ppm
P_8W_{48} from ref 27	−190.1
	−191.0
	−207.6
perp-$[K_8(Mo^{VI}O_2)_2(Mo^{V}_4O_{10}(H_2O)_3)(P_8W_{48}O_{184})]^{25-}$ from ref 27	−137.1
	−190.5
	−193.0
	−205.7
	−215.6
	−304.4
NaK-2	−165.0
	−174.7
	−197.1
	−201.1
	−205.9
	−211.3
	−222.4
Na-2	−196.3
	−200.9
	−221.8

dx.doi.org/10.1021/ic202346r | *Inorg. Chem.* 2012, 51, 2349−2358

EDX atomic ratio calculated for $Na_{28}H_8[\{Mo_4O_4S_4(OH)_2(H_2O)_3\}_2(P_8W_{48}O_{184})]\cdot 130H_2O\cdot\sim 8$ NaCl (found): W/Mo = 6.0 (6.12); Mo/S = 1 (1.03); P/Mo = 1 (1.09); W/Na = 1.33 (1.37); absence or only traces of potassium.

RESULTS AND DISCUSSION

Structure. Compound **1** crystallizes as a mixed potassium–lithium salt in the tetragonal space group *I*4/*mmm*. The molecular arrangement in **1** corresponds to a P_8W_{48} macrocyclic ring capped on both sides by two disordered $[Mo_4O_4S_4(OH)_2(H_2O)_3]^{2+}$ oxothiomolybdenum clusters (Figure 1). On each side, the $[Mo_4O_4S_4(OH)_2(H_2O)_3]^{2+}$ hemicycle appears distributed with a statisticall occupancy factor of 50% over two equivalent positions related through a C_4 symmetry axis. Such disorder can be analyzed through two different options. The first one consists in the presence of two positional isomers located on the same crystallographic site and was characterized by the relative disposition perpendicular (noted *perp*) or parallel (noted *para*) of the two $[Mo_4O_4S_4(OH)_2(H_2O)_3]^{2+}$ (Figure 1) groups. The second way could result from a positional disorder of a single isomer (either *perp* or *para*). Overall, ^{31}P NMR studies in solution and the solid state performed on parent compound **2** (see below) are consistent with the presence of two anions and then corresponding to the *perp* and *para* isomers. Then, the observed crystallographic disorder has to be properly analyzed according to the first option, as depicted in Figure 1. In the structure of **1**, the tetranuclear "basket handle" core results from the connection of two $\{Mo_2O_2S_2\}$ groups through face-shared octahedra, involving two bridging hydroxo groups and a water molecule (Mo···Mo = 3.317 Å, Mo···$OH_{bridging}$ = 2.116 Å, Mo···$OH_{2\ bridging}$ = 2.536 Å). In addition, the coordination sphere of the two peripheral Mo atoms of the tetranuclear arch is completed by a terminal inward directed aquo ligand (Mo···OH_2 = 2.331 Å) to give octahedral Mo(V) centers. Such a tetranuclear fragment was already observed in the supramolecular assembly formed by combination of $[Mo_2O_2S_2]^{2+}$ and P_2W_{15}[37] and in the coordination compound $[Mo_4S_4O_4(OH)_2(H_2O)_3(pba)]^{2-}$.[41] The molecular structure of **1** closely ressembles the fully oxo analogue previously described by Müller et al.,[27] which represents the unique example where the oxo cation $\{Mo_2O_4\}^{2+}$ exhibits a similar mode of junction as those usually observed for the oxothio $\{Mo_2O_2S_2\}$-based molecules. Nevertheless, both tetranuclear arrangements, oxo versus oxothio, differ slightly by their protonation degree, although both complexes were synthetized in the same pH range. The oxo derivative results in connections between both dinuclear units through a double oxo bridge, giving the neutral core $[Mo^V_4O_{10}(H_2O)_3]$, while such connections are ensured trough a double hydroxo bridge within the oxothio derivative. Such a difference arises probably from the softening of the Mo centers though the presence of the double sulfido bridge, which weakens and stretches significantly the trans Mo–O bonds. Such a Mo-softening effect found expression in differing self-condensation properties, which lead to exclusively cyclic linear oligomers with $\{Mo_2O_2S_2\}^{2+}$ [42] and compact stacked arrangements with $\{Mo_2O_4\}^{2+}$.[43] In these specific cases the common mode of junction of dimolybdic units could be due to a vectorial growth of the self-condensation process, which is strongly directed by the coordination requirement of the P_8W_{48} macrocycle. The tetranuclear arches are grafted on the anion surface through W–O–Mo bridges (Mo···O = 2.148 Å) (see Figure 2). As commonly observed for P_8W_{48} derivatives,[9,23,25–27] four potassium cations are found inside the cavity, statistically distributed over four pairs of equivalent sites (SOF = 50%) which span two neighboring P_2W_{12} subunits with the usual K–O bonds (2.736–2.795 Å) (see Figures 3 and 4). In addition, a weak electronic density was found very close to the peripheral Mo atom and matches with that corresponding to 1/8 tungsten atoms. Such a result is consistent with previous results which show that these one-eighth equivalent positions are able to coordinate cis dioxo metallic cation $\{MO_2\}$ with M = Mo, W, or V.[20,22,24,25,27] This W atom is bound to two oxygen atoms of two adjacent P_2W_{12} units (W···O = 1.754 Å) and two terminal cis oxygen atoms (W···O = 1.781 and 1.901 Å), which complete the distorted tetrahedral environment. Obviously, the $\{WO_2\}^{2+}$ group is coordinated on the four coordination sites remaining free within the *para* and *perp* isomers (see Figure 3 and 4), giving in such conditions one $\{WO_2\}^{2+}$ group per isomer (*para* and *perp*).

Synthesis of the Compounds. ^{31}P NMR solution study (not shown) reveals that **1** is not a pure compound. As surmised, the presence of one $\{WO_2\}^{2+}$ group distributed over two isomers and disordered over four positions in each isomer could produce several compounds. As invoked by Kortz et al., the additional cis dioxotungstic group is most likely formed during synthesis of the P_8W_{48} derivatives, which can require prolonged heating.[23,25,20] Under such conditions, the degradation process of P_8W_{48} results in release of oxo–tungstic species able to react further on the P_8W_{48} precursor. Herein, the ^{31}P NMR and UV–vis studies of the $\{Mo_2O_2S_2\}/P_8W_{48}$ systems reveal that formation of the *para* and *perp* isomers is quantitative and proceeds fast at room temperature. Then, no heating is required to produce the addition compound. Actually, prolonged heating used for the synthesis of **KLi-1** allows only the increase of the crystal quality required for X-ray diffraction. Optimized synthetic procedures, carried out at room temperature, allows isolating *perp/para* isomers as mixed K–Li (compound **KLi-2**) or K–Na–Li salts (compound **NaK-2**).

NMR Studies. *Characterization of Compound 2.* ^{31}P NMR data of compounds **KLi-2**, **NaK-2**, and **Na-2** are reported in Table 2. The ^{31}P NMR spectrum of mixed potassium–lithium salt **KLi-2** in 1 M LiCl, depicted in Figure 5b, consists of three resolved lines located at −7.54, −8.18, and −8.92 ppm. It differs significantly from that of the free P_8W_{48} precursor,

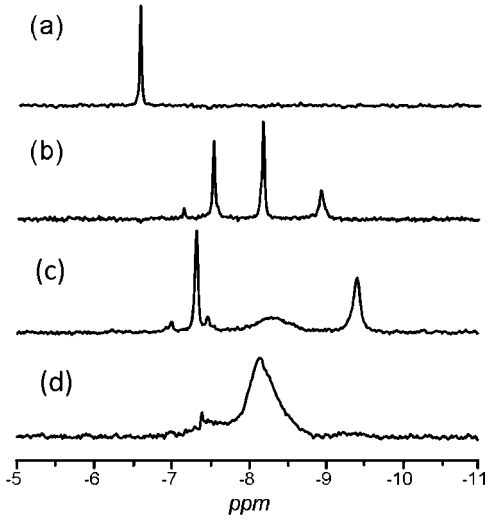

Figure 5. ^{31}P NMR spectra of compounds P_8W_{48} (a), **KLi-2** (b), **NaK-2** (c), and **Na-2** (d) in aqueous LiCl (1 M).

dx.doi.org/10.1021/ic202346r | Inorg. Chem. 2012, 51, 2349–2358

which gives a single resonance at −6.56 ppm (see Figure 5a). The three resonances are attributed to a mixture of the two isomers, namely, *para*- and *perp*-$[\{Mo_4O_4S_4(OH)_2(H_2O)_3\}_2P_8W_{48}]^{36-}$ (Figures 3 and 4). The *parallel* arrangement should retain a nominal D_{2h} symmetry, giving the two ^{31}P NMR signals of equal intensities observed at −7.54 and −8.92 ppm, while the *para* isomer gives the single resonance at −8.18 ppm, related to the four equivalent phosphate groups within the D_{2d} idealized symmetry. For both isomers, the $\{Mo_2O_2S_2\}$ coordination of the P_8W_{48} surface is characterized by a significant shielding at the ^{31}P nuclei. In the *para* isomer, one pair of equivalent phosphates is located far from the two $[Mo_4O_4S_4(OH)_2(H_2O)_3]^{2+}$ handles and then could correspond to the high-frequency resonance at −7.54 ppm, while the remaining pair, sited in the vicinity of both *para*-arranged $[Mo_4O_4S_4(OH)_2(H_2O)_3]^{2+}$ handles, could be assigned to the low-frequency line at −8.92 ppm. Interestingly, the low-frequency resonance at −8.92 ppm appears significantly broadened ($\Delta\nu_{1/2}$ = 12 Hz) compared to the other ($\Delta\nu_{1/2}$ = 3 Hz). Such an observation could be related to a mutual trans influence of the two parallel $[Mo_4O_4S_4(OH)_2(H_2O)_3]^{2+}$ handles, which spread along the W−O−W bridges. In agreement with such an attribution, the four equivalent phosphates within the *perp* isomer are close to only one $[Mo_4O_4S_4(OH)_2(H_2O)_3]^{2+}$ handle and far from the second, thus giving a resonance observed at −8.18, about halfway between −7.54 and −8.92 ppm. Besides, this ^{31}P NMR chemical shift appears in good agreement with that found for$[(VO_2)_4(P_8W_{48}O_{184})]^{36-}$ (δ = −8.1 ppm) which exhibits a similar distribution of the four $\{VO_2\}^+$ within the cavity.[20] The ratio of both isomers in **KLi-2** calculated from integrated ^{31}P NMR lines gives values around 55 ± 5% for the *perp* isomer vs 45 ± 5% for the *para* compound. Such an observation is consistent with a slightly unfavorable trans influence for the *para* isomer with respect to the *perp* arrangement. The *perp*/*para* ratio does not vary significantly neither with time nor with temperature in the 275−345 K range. Evidence of two isomers for such a system, i.e., $\{Mo_2O_2S_2\}$-containing P_8W_{48}, contrasts clearly with results obtained by Müller et al. about the oxo derivative $[K_8(MoO_2)_4(Mo_4O_{10}(H_2O)_3)_2(P_8W_{48}O_{184})]^{24-}$.[27] The latter gives only a single sharp ^{31}P NMR resonance, consistent with the presence of the perpendicular arrangement as a single isomer.[27]

The ^{31}P NMR spectrum of the mixed sodium−potassium−lithium salt **NaK-2** in 1 M LiCl (Figure 5c) differs significantly, revealing that chemical shifts and line widths are quite sensitive to the nature of the embedded countercations (see Table 2). In **NaK-2**, the separation of two signals corresponding to the *para* isomer appears significantly more important ($\Delta\delta$ = 2.1 ppm) while their line width remains unchanged. The ^{31}P NMR resonance of the *perp* isomer remarkably broadens from 3 Hz in **KLi-2** to 56 Hz in **NaK-2**, and the ratio *perp*/*para* is reversed to give 0.3/0.7. This result suggests that the nature and distribution of the enclosed countercations have a significant influence upon the charge density by the coordinating oxygen atoms lining both sides of the P_8W_{48} cavity. Furthermore, the variation of the ^{31}P NMR line width from 3 to 56 Hz, observed for the *perp*-isomer, indicates that dynamics is strongly influenced by the nature of the counterion K^+ versus Na^+ and by the nature of the isomer. Several pathways for dynamics can be postulated, such as cation exchange from the cavity to the solvent or intramolecular exchange involving the four pairs of sites identified by X-ray diffraction (see above). Interestingly, addition of 5−10 equiv of KCl to a solution of **NaK-2** leads to a sharpening of the ^{31}P NMR resonance of the *perp* isomer and allows recovering an overall ^{31}P spectrum close to **KLi-2** (see Figure S1, Supporting Information). Such results suggest that in the enriched Na^+ salt **NaK-2** the cavity encloses the sodium cation, which is labile enough to be replaced by potassium. The strongest affinity of the cavity for the potassium is related to the size requirement of the eight sites which exhibit in the solid state seven K−O distances in the 2.73(2)−2.79 Å range.[9] From these considerations it seems consistent to consider faster exchange rates with the smallest cations such as sodium. The simplest dynamics could be viewed as intramolecular hopping of each inner cation within the four pairs of sites, where both sites are separated by a short distance of 2.48(2) Å. Within the *para* isomers these four pairs are composed of two equivalent sites, leading to a strictly equal averaged distribution of the sodium cations through a fast hopping. In the *perp* isomer, these sites become inequivalent, which could result in a lower hopping frequency of the sodium cation on the NMR time scale, experimentally observed as a broad ^{31}P NMR resonance. The potassium-free compound **Na-2** which correspond to the second crop of crystallization in the synthesis of **NaK-2** is characterized by very broad ^{31}P NMR peaks which likely involves both isomers i.e., *perp* compound (δ = −8.15 ppm; $\Delta\nu_{1/2}$ = 55 Hz) and *para* species (δ = −7.3 ppm, $\Delta\nu_{1/2} \approx$ 35 Hz and −8.95 ppm; $\Delta\nu_{1/2} \approx$ 60 Hz). The ^{31}P NMR spectrum of **Na-2** features typical signals at the limit of the coalescence and then suggests that in the absence of potassium ion both isomers are related through a dynamic equibrium involving a decoordination/coordination process of the two $[Mo_4O_4S_4(OH)_2(H_2O)_3]^{2+}$ handles. Furthermore, quantitative analysis of the ^{31}P NMR spectrum indicates that **Na-2** contains about 85% *perp* isomer. The ^{31}P NMR spectrum of an aged solution of **Na-2** (1 month later) does not show any significant changes in the isomeric *perp*/*para* ratio (see Figure S2, Supporting Information), thereby evidencing an equilibrium state. As previously mentioned, addition of small amounts of KCl to a solution of **Na-2** (5−10 equiv) provokes an important sharpening of the middle peak from 55 to 12 Hz (see Figure S3, Supporting Information) previously attributed to the *perp* isomer, but surprisingly, the low-frequency resonance assigned to one phosphate group within the *para* isomer disappears, probably due to a substantial broadening, while the other resonance of the *para* species remains unchanged. Furthermore, the ratio *perp*/(*para* + *perp*) decreases slightly from 85% to 65%. These qualitative results show that the nature of the counterion Na^+ vs K^+ has a great influence upon (i) the relative stability of both isomers and (ii) the dynamic exchange of the intramolecular cation with a significant effect on the lability of the two $[Mo_4O_4S_4(OH)_2(H_2O)_3]^{2+}$ handles grafted on the P_8W_{48} surface.

In addition to the solution studies, compounds **NaK-2** and **Na-2** were characterized by solid-state ^{31}P NMR. ^{31}P MAS NMR spectra (see Figure S4, Supporting Information) exhibit a large peak which results from the overlap of the three resonances related to the presence of both isomers. ^{31}P MAS NMR of compound **Na-2** reveals only one signal with symmetric shape at −9.5 ppm which could be related to the resonance of the *perp* isomer as the predominant species. Conversely, the compound **NaK-2** reveals a large asymmetric signal characterized by a peak maximum at −8.3 ppm and a shoulder at −9.7 ppm. Such an asymmetric shape could be due to the presence of both isomers and can be analyzed as follows: these two chemical shifts, i.e., −8.3 and −9.7 ppm, could correspond to the two expected equal lines of the *para* isomer, while the additional contribution of the *perp* isomer could be found close to −8.7 ppm. Deconvolution of both lines at −8.3 and −9.7 ppm

dx.doi.org/10.1021/ic202346r | *Inorg. Chem.* 2012, 51, 2349−2358

gives an integrated intensity ratio of about 70/30, which leads to a proportion of about 40% for the *perp* isomer and 60% for the *para* species. Such values appear in agreement with the isomeric distribution found in solution (see Table 2).

Compounds **NaK-2** and **Na-2** have been also characterized by their ^{183}W NMR spectra, shown in Figures 6 and S5, Supporting Information. ^{183}W NMR data are given in Table 3. Surprisingly, ^{183}W NMR spectra of **NaK-2** and **Na-2** are very different. The spectrum of **NaK-2** exhibits seven ^{183}W NMR broad resonances, while that of **Na-2** reveals only three equal broad signals at −196.3, −200.9, and −221.8 ppm. Furthermore, it is noteworthy that ^{183}W NMR spectra of both **NaK-2** and **Na-2** contrast clearly with that obtained from the oxo derivative *perp*-$[K_8(Mo^{VI}O_2)_4(Mo^{V}_4O_{10}(H_2O)_3)(P_8W_{48}O_{184})]^{24-}$, where the six sharp ^{183}W NMR lines were fully consistent with the structure found by X-ray crystallography.[27] In the case of the $\{Mo_2O_2S_2\}$-containing P_8W_{48} derivatives, the presence of the two isomers *perp* and *para* involved in dynamic processes have to be considered. The presence of three ^{183}W NMR equal resonances for **Na-2** indicates an apparent D_{4h} symmetry for the P_8W_{48} skeleton, while lower symmetries D_{2d} *and* D_{2h} are expected for the frozen isomers *perp* and *para*, respectively. Then the D_{4h} symmetry must necessarily correspond to an averaged symmetry, arising from a dynamic process where the *para* and *perp* species are the limiting structures. Such a process can be viewed as the fast wheeling of both $[Mo_4O_4S_4(OH)_2(H_2O)_3]^{2+}$ handles on opposite faces of P_8W_{48}. Such a dynamic process was already postulated from analysis of the ^{31}P NMR data of **Na-2** because the broad signals attributed to the *para* and *perp* isomers were at the limit of coalescence. The ^{183}W NMR spectrum of **NaK-2** appears more complex because the seven observed ^{183}W NMR lines should be the contribution of both isomers, although theoretically two sets of six resonances are expected. Actually, accidental degeneracy can occur because in both isomers some tungsten atoms retain very close chemical environments. ^{183}W and ^{31}P NMR studies lead to the univocal conclusion that the nature of the inner alkali cation governs to some extent the interconversion rate between *para*/*perp* isomers and even influences the isomeric ratio at the equilibrium. Both related effects arise from very weak coordination bonds between the two $\{Mo_4S_4(OH)_2(OH_2)_3\}$ "handles" and the P_8W_{48} macrocycle. The weakness of POM-$\{Mo_2O_2S_2\}$ connections was already evidenced for dimeric assemblies $[(PW_{11})_2(H_4Mo_4S_4O_6)]^{10-}$ and $[(P_2W_{17})_2(H_4Mo_4S_4O_6)]^{16-}$,[36,38] which isomerize easily in cisoid or transoid species. In the present case, this behavior allows direct control of the coordination/decoordination processes induced by the inner countercations.

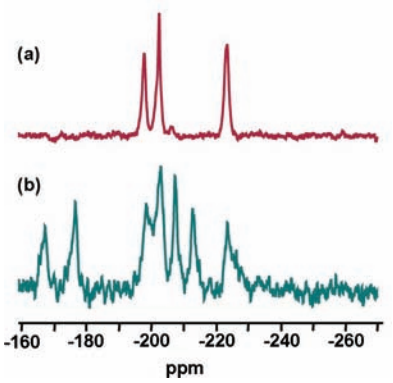

Figure 6. ^{183}W NMR spectra of compounds **Na-2** (a) and **NaK-2** (b) in aqueous LiCl (1 M).

^{31}P NMR Titrations. Batch ^{31}P NMR titrations of P_8W_{48} by $[Mo_2O_2S_2]^{2+}$ in aqueous medium were performed at pH = 1, 2, 3, and 4.7 after exchanging of the main part of potassium cations for sodium to increase solubility. Figure 7 shows the results obtained at pH = 3, whereas the titrations carried out at pH = 1, 2, and 4.7 are depicted in Figure S6, Supporting Information. In all titration experiments addition of $[Mo_2O_2S_2]^{2+}$ to P_8W_{48} causes initially growing of two signals of the same intensities in the −7.7 to −8.4 ppm range, whereas the signal of free P_8W_{48} decreases. Intensities of these two signals are maximum for ratio $[Mo_2O_2S_2]^{2+}/P_8W_{48} = 2$. For higher ratios, these two lines decrease gradually together for the benefit of the signals corresponding to the saturated adducts, distributed as *para* and *perp* isomers. Up to ratio $[Mo_2O_2S_2]^{2+}/P_8W_{48} = 4$, ^{31}P NMR spectra do not change significantly (not shown) and consist mainly of the three resonances attributed to the *para* and *perp* isomers. As suggested by the stoichiometry and the feature of the ^{31}P NMR spectra, the two signals found in the −7.7 to −8.4 ppm range have to be assigned to an intermediate, consistent with the "monohandle" derivative $[\{Mo_4O_4S_4(OH)_2(H_2O)_3\}P_8W_{48}]^{38-}$.

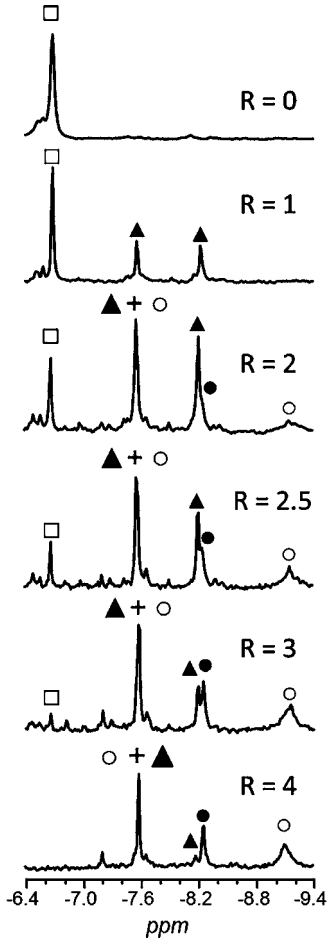

Figure 7. ^{31}P NMR titrations of P_8W_{48} by $[Mo_2O_2S_2]^{2+}$ in aqueous LiCl medium at pH = 3. Ratio *R* corresponds to the ratio $[Mo_2O_2S_2]^{2+}/P_8W_{48}$. P_8W_{48} (□), intermediate compound $[\{Mo_4O_4S_4(OH)_2(H_2O)_3\}P_8W_{48}]^{38-}$ (▲), *para*-$[\{Mo_4O_4S_4(OH)_2(H_2O)_3\}_2P_8W_{48}]^{36-}$ (○), and *perp*-$[\{Mo_4O_4S_4(OH)_2(H_2O)_3\}_2P_8W_{48}]^{36-}$ (●).

dx.doi.org/10.1021/ic202346r | *Inorg. Chem.* 2012, 51, 2349−2358

In such conditions, the preferential formation of the *para* isomer is observed (*para*/(*para* + *perp*) ≈ 80%). From the ^{31}P NMR spectra and their interpretations the speciation curve can be obtained and are shown in Figure 8. In summary, ^{31}P NMR

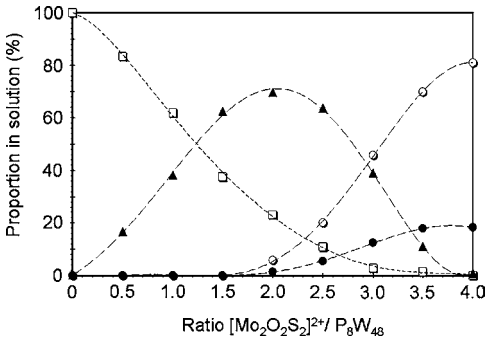

Figure 8. Speciation curve obtained for the ^{31}P NMR titration performed at pH = 3: P_8W_{48} (□), intermediate compound $[\{Mo_4O_4S_4(OH)_2(H_2O)_3\}P_8W_{48}]^{38-}$ (▲), *para*-$[\{Mo_4O_4S_4(OH)_2(H_2O)_3\}_2P_8W_{48}]^{36-}$ (○), and *perp*-$[\{Mo_4O_4S_4(OH)_2(H_2O)_3\}_2P_8W_{48}]^{36-}$ (●).

titrations allowed (i) evidencing formation of an intermediate consistent to the monohandle derivative $[\{Mo_4O_4S_4(OH)_2(H_2O)_3\}P_8W_{48}]^{38-}$ and (ii) identifying preferential formation of *para*-$[\{Mo_4O_4S_4(OH)_2(H_2O)_3\}_2P_8W_{48}]^{36-}$ (80%) over the *perp*-$[\{Mo_4O_4S_4(OH)_2(H_2O)_3\}_2P_8W_{48}]^{36-}$ isomer (20%).

Spectrophotometric Studies. Batch spectrophotometric titrations of a $[Mo_2O_2S_2]^{2+}$ solution with P_8W_{48} were performed in 1 M LiCl at pH = 1.5, 3, and 4.7. The results obtained at pH = 3 are shown in Figure 9, whereas titrations at

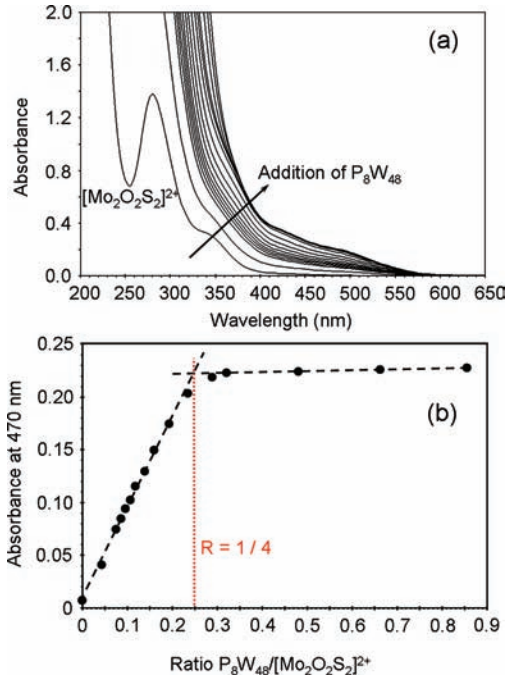

Figure 9. UV−vis titration of $[Mo_2O_2S_2]^{2+}$ by P_8W_{48} in aqueous LiCl medium at pH = 1. Evolution of the resulting spectrum upon addition of increasing amounts of P_8W_{48} (a). Variation of the absorbance measured at 470 nm as a function of the ratio $R = P_8W_{48}/[Mo_2O_2S_2]^{2+}$.

pH = 1.5 and 4.7 are shown in the Supporting Information (Figures S7 and S8). Absorptions in the 420−500 nm range are characteristic of the red-brown thioderivatives of POMs[32,34,36−38] since $\{Mo_2O_2S_2\}$-based species[31] and P_8W_{48} alone do not exhibit significant absorptions in this region. Gradual addition of P_8W_{48} to a constant quantity of $[Mo_2O_2S_2]^{2+}$ leads to gradual increasing of the absorbance in this region until a break point at $P_8W_{48}/[Mo_2O_2S_2]^{2+}$ = 1/4, consistent with the stoichiometry of the saturated complex (Figure 9b). Similar results are obtained at pH = 1.5 and 4.7 (Figures S7 and S8, Supporting Information), thus confirming binding of four oxothiocations $[Mo_2O_2S_2]^{2+}$ per one P_8W_{48} in diluted solutions.

Stability and Electrochemistry Studies. Stability studies in solution as a function of pH (from 1 to 5) were done by UV−vis spectroscopy and cyclic voltammetry. The stability criterion was reproducibility for spectra and cyclic voltammograms (CVs) after several hours of running experiments. We found that compounds P_8W_{48}, **KLi-1**, and **Na-2** were stable enough in sulfate buffer solution from pH 1 to 3 (0.5 M Li_2SO_4 + H_2SO_4) to be characterized by cyclic voltammetry. It was therefore possible and easy to draw direct comparison between their respective electrochemical behaviors in solution.

Figure 10 compares **Na-2** and P_8W_{48} CVs recorded under the same conditions (0.5 M Li_2SO_4 + H_2SO_4/pH = 2.0;

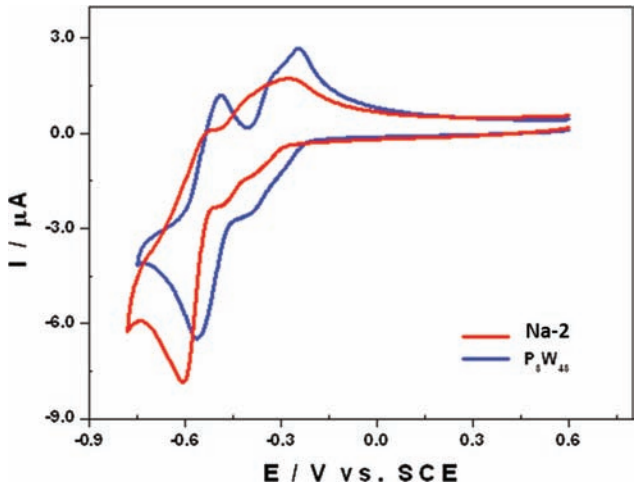

Figure 10. Cyclic voltammograms of **Na-2** (red) and $\mathbf{P_8W_{48}}$ (blue) in 0.5 M Li_2SO_4, pH = 2. Scan rate of 10 mV·s^{-1}; working electrode glassy carbon. Potentials are quoted against SCE reference electrode. POM concentrations = 0.2 mM.

scan rate 10 mV s^{-1}). The CV of **Na-2** is characterized by three reduction steps located at −0.38, −0.47, and −0.61 V versus SCE reference electrode. Compared to P_8W_{48} reduction peaks, there is a potential shift of 80, 70, and 50 mV for the first, second, and third reduction steps, respectively, at each time in favor of P_8W_{48} reduction (see Table 4). These differences

Table 4. Reduction Peak Potentials, E_{pc}, for the First and Second Tungsten Waves Determined by Cyclic Voltammetry at pH 1, 2, and 3 for Compounds Na-2 and P_8W_{48}[a]

	pH = 1		pH = 2		pH = 3	
	E_{pc_1}	E_{pc_2}	E_{pc_1}	E_{pc_2}	E_{pc_1}	E_{pc_2}
Na-2	−0.29	−0.40	−0.38	−0.47	−0.45	−0.53
$\mathbf{P_8W_{48}}$	−0.20	−0.30	−0.30	−0.40	−0.40	−0.49

[a]Scan rate 10 mV·s^{-1}, working electrode glassy carbon, reference electrode SCE.

dx.doi.org/10.1021/ic202346r | Inorg. Chem. 2012, 51, 2349−2358

observed at pH = 2 could suggest a higher basicity and/or a higher formal negative charge for **Na-2** as compared to P_8W_{48} under such conditions.

Another characteristic that merited special study is the number of electrons exchanged in each redox step. It is well established that P_8W_{48} is a real electron sink (8 electrons for the two first waves and 8 for the third one).[44] Controlled potential coulometry experiments were carried out on a solution of **Na-2** in 0.5 M Li_2SO_4 + H_2SO_4/pH = 3.00. With the working electrode potential set at −0.55 V vs SCE (first two reduction steps) the electrical charge that flows through the solution corresponded to an average of 8.3 ± 0.1 mol of electrons consumed per mole of **Na-2**. This value is consistent with reduction of the tungstic framework of P_8W_{48}. When the potential is set at −0.72 V vs SCE, i.e., on the third wave, the number of electrons per mole of **Na-2** is much higher than the expected 16 mol. This difference is certainly due the electrocatalytic reduction of protons that takes place here. This explains the magnitude of this third reduction wave and its irreversible nature, as compared to the same wave for P_8W_{48} (Figures 10 and S9, Supporting Information). Indeed, one can list at least three conditions that, when combined, would promote this phenomenon: the pH of the medium (3.00), the relative low potential (−0.72 V vs SCE), and the presence of two $\{Mo_4O_4S_4\}$ entities which in many cases are described as good electrocatalysts for H^+ reduction.[29−31] The presence of these two $\{Mo_4O_4S_4\}$ entities is also highlighted by an irreversible oxidation wave that appears above +0.65 V vs SCE at pH 3 (see Figure S10, Supporting Information). For comparison, the CV of the molybdenum "wheel" $[Mo_8S_8O_8(OH)_8(C_2O_4)]^{2-}$ recorded under the same conditions displays an irreversible wave with an oxidation peak potential located at +0.88 V vs SCE (see Figure S10, Supporting Information), which could be assigned to irreversible oxidation of Mo^V into Mo^{VI}.

In aqueous solution, the redox behavior of **Na-2** is pH dependent, as seen in Figure 11. As the pH of the electrolyte

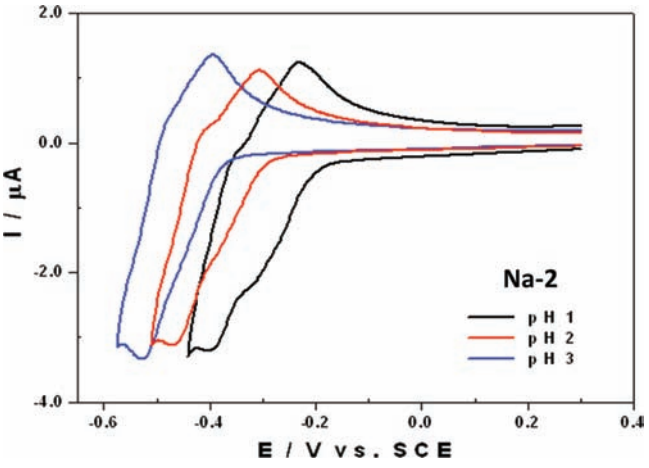

Figure 11. Cyclic voltammograms of **Na-2** at different pH values: pH 1 (black), 2 (red), and 5 (blue). Polyoxometalate concentration 0.2 mM; scan rate 10 $mV{\cdot}s^{-1}$; working electrode: glassy carbon; reference electrode SCE.

increases from 1 to 3, the reduction waves are shifted in the direction of positive potentials but no noticeable change of their shape is observed. Table 4 summarizes reduction peak potential values for the first and second waves of **Na-2** in 0.5 M Li_2SO_4 at pH 1, 2, and 3.

CONCLUSION

This study was devoted to the reactivity of the superlacunary P_8W_{48} with the oxothiocation $[Mo_2O_2S_2]^{2+}$ in aqueous medium. Solution studies, carried out by ^{31}P and ^{183}W NMR and UV−vis spectroscopy, demonstrate that coordination of $\{Mo_2S_2O_2\}$ on P_8W_{48} leads to an intermediate, corresponding probably to the monohandle derivative prior to formation of the saturated adducts. A structural model has been established by X-ray diffraction study showing a structural disorder explained by superimposition of both geometrical *para* and *perp* isomers. Moreover, the influence of the countercations K^+ versus Na^+ upon the equilibrium state and the dynamic properties of the saturated bishandle derivatives was also demonstrated qualitatively. The $\{Mo_2O_2S_2\}$-containing P_8W_{48} anions represent relevant chemical models to study the internal distribution of cation in solution, crucial for understanding the host−guest properties of the large macrocyclic anion P_8W_{48}. A quantitative study of the host−guest properties of the $\{Mo_2O_2S_2\}$-P_8W_{48} derivatives is under investigation using multinuclear NMR methods (^{23}Na, ^{39}K, ^{7}Li).

ASSOCIATED CONTENT

Supporting Information

^{31}P NMR spectra of **NaK-2** in aqueous 1 M LiCl without addition of KCl and after addition of 5 and 10 equiv of KCl (Figure S1); ^{31}P NMR spectra of compound **Na-2** in aqueous 1 M LiCl recorded after 1 month compared to a spectrum recorded just after preparation of the NMR tube (Figure S2); ^{31}P NMR spectra of the sodium salt **Na-2** in aqueous 1 M LiCl without addition of KCl and after addition of 10 equiv of KCl (Figure S3); ^{31}P MAS NMR spectra of compounds **KLi-2**, **NaK-2**, and **Na-2** in the solid state (Figure S4); simulated ^{183}W NMR spectra of **NaK-2** in aqueous 1 M LiCl (Figure S5); ^{31}P NMR titrations of P_8W_{48} by $[Mo_2O_2S_2]^{2+}$ in aqueous LiCl medium at pH = 2 and 4.7 (Figure S6); results of the UV−vis titration of $[Mo_2O_2S_2]^{2+}$ by P_8W_{48} in aqueous LiCl medium at pH = 1.5 and 4.7 (Figures S7 and S8); cyclic voltammograms of **Na-2** and **P_8W_{48}** in 0.5 M Li_2SO_4 + H_2SO_4 pH 3 between −0.8 and +1.4 V (Figure S9); cyclic voltammograms of $[Mo_8O_8S_8(OH)_8(C_2O_4)]^{2-}$ in 0.5 M Li_2SO_4 + H_2SO_4 at pH 3 (Figure S10); X-ray crystallographic data in CIF format. This material is available free of charge via the Internet at http://pubs.acs.org.

AUTHOR INFORMATION

Corresponding Author

*E-mail: sebastien.floquet@chimie.uvsq.fr (S.F.); cadot@chimie.uvsq.fr (E.C.).

ACKNOWLEDGMENTS

We gratefully acknowledge the Centre National de la Recherche Scientifique (CNRS) and the Ministère de l'Education Nationale de l'Enseignement Supérieur et de la Recherche (MENESR) for their financial support. S.F. is grateful to Mr. Jimmy Mercier and Mr. Duc-Nam Luu for their contributions to the experimental work. We are also grateful to the GDRI Suprachem and the French Ministery of Foreign Affairs for their support through the Ph.D. grant for V.S.K. This work was also supported by the National Research Agency (ANR) under contract POMEAH·ANR-08-JCJC-0097. The work was supported by Russian Foundation for Basic Research (Grant 09-03-93105).

REFERENCES

(1) Proust, A.; Thouvenot, R.; Gouzerh, P. *Chem. Commun.* **2008**, *16*, 1837−1852.
(2) Ogata, A.; Yanagie, H.; Ishikawa, E.; Morishita, Y.; Mitsui, S.; Yamashita, A.; Hasumi, K.; Takamoto, S.; Yamase, T.; Eriguchi, M. *Br. J. Cancer* **2008**, *98* (2), 399−409.
(3) Kortz, U.; Müller, A.; van Slageren, J.; Schnack, J.; Dalal, N. S.; Dressel, M. *Coord. Chem. Rev.* **2009**, *253* (19−20), 2315−2327.
(4) Mialane, P.; Dolbecq, A.; Sécheresse, F. *Chem. Commun.* **2006**, *33*, 3477−3485.
(5) Miras, H. N.; Cooper, G. J. T.; Long, D. L.; Bogge, H.; Müller, A.; Streb, C.; Cronin, L. *Science* **2010**, *327* (5961), 72−74.
(6) Ritchie, C.; Cooper, G. J. T.; Song, Y. F.; Streb, C.; Yin, H. B.; Parenty, A. D. C.; MacLaren, D. A.; Cronin, L. *Nat. Chem.* **2009**, *1* (1), 47−52.
(7) Pradeep, C. P.; Misdrahi, M. F.; Li, F. Y.; Zhang, J.; Xu, L.; Long, D. L.; Liu, T. B.; Cronin, L. *Angew. Chem., Int. Ed.* **2009**, *48* (44), 8309−8313.
(8) Rodriguez-Albelo, L. M.; Ruiz-Salvador, A. R.; Sampieri, A.; Lewis, D. W.; Gomez, A.; Nohra, B.; Mialane, P.; Marrot, J.; Sécheresse, F.; Mellot-Draznieks, C.; Biboum, R. N.; Keita, B.; Nadjo, L.; Dolbecq, A. *J. Am. Chem. Soc.* **2009**, *131* (44), 16078−16087.
(9) Contant, R.; Tézé, A. *Inorg. Chem.* **1985**, *24* (26), 4610−4614.
(10) Mal, S. S.; Bassil, B. S.; Ibrahim, M.; Nellutla, S.; van Tol, J.; Dalal, N. S.; Fernandez, J. A.; Lopez, X.; Poblet, J. M.; Biboum, R. N.; Kelta, B.; Kortz, U. *Inorg. Chem.* **2009**, *48* (24), 11636−11645.
(11) Chen, L. F.; Hu, J. C.; Mal, S. S.; Kortz, U.; Jaensch, H.; Mathys, G.; Richards, R. M. *Chem.—Eur. J.* **2009**, *15* (30), 7490−7497.
(12) Bao, Y. Y.; Bi, L. H.; Wu, L. X.; Mal, S. S.; Kortz, U. *Langmuir* **2009**, *25* (22), 13000−13006.
(13) Liu, G.; Liu, T. B.; Mal, S. S.; Kortz, U. *J. Am. Chem. Soc.* **2006**, *128* (31), 10103−10110.
(14) Alam, M. S.; Dremov, V.; Muller, P.; Postnikov, A. V.; Mal, S. S.; Hussain, F.; Kortz, U. *Inorg. Chem.* **2006**, *45* (7), 2866−2872.
(15) Mal, S. S.; Kortz, U. *Angew. Chem., Int. Ed.* **2005**, *44* (24), 3777−3780.
(16) Jabbour, D.; Keita, B.; Nadjo, L.; Kortz, U.; Mal, S. S. *Electrochem. Commun.* **2005**, *7* (8), 841−847.
(17) Pichon, C.; Mialane, P.; Dolbecq, A.; Marrot, J.; Rivière, E.; Keita, B.; Nadjo, L.; Sécheresse, F. *Inorg. Chem.* **2007**, *46* (13), 5292−5301.
(18) Mal, S. S.; Dickman, M. H.; Kortz, U.; Todea, A. M.; Merca, A.; Bogge, H.; Glaser, T.; Müller, A.; Nellutla, S.; Kaur, N.; van Tol, J.; Dalal, N. S.; Keita, B.; Nadjo, L. *Chem.—Eur. J.* **2008**, *14* (4), 1186−1195.
(19) Mitchell, S. G.; Gabb, D.; Ritchie, C.; Hazel, N.; Long, D. L.; Cronin, L. *CrystEngComm* **2009**, *11* (1), 36−39.
(20) Bassil, B. S.; Ibrahim, M.; Mal, S. S.; Suchopar, A.; Biboum, R. N.; Keita, B.; Nadjo, L.; Nellutla, S.; van Tol, J.; Dalal, N. S.; Kortz, U. *Inorg. Chem.* **2010**, *49* (11), 4949−4959.
(21) Mitchell, S. G.; Boyd, T.; Haralampos, N. M.; De-Liang, L.; Cronin, L. *Inorg. Chem.* **2011**, *50*, 136−143.
(22) Chen, S.-W.; Boubekeur, K.; Gouzerh, P.; Proust, A. *J. Mol. Struct.* **2011**, *994*, 104−108.
(23) Zimmermann, M.; Belai, N.; Butcher, R. J.; Pope, M. T.; Chubarova, E. V.; Dickman, M. H.; Kortz, U. *Inorg. Chem.* **2007**, *46* (5), 1737−1740.
(24) Zhang, J.; Liu, T. B.; Mal, S. S.; Kortz, U. *Eur. J. Inorg. Chem.* **2010**, *20*, 3195−3200.
(25) Mal, S. S.; Nsouli, N. H.; Dickman, M. H.; Kortz, U. *Dalton Trans.* **2007**, *25*, 2627−2630.
(26) Müller, A.; Pope, M. T.; Todea, A. M.; Bogge, H.; van Slageren, J.; Dressel, M.; Gouzerh, P.; Thouvenot, R.; Tsukerblat, B.; Bell, A. *Angew. Chem., Int. Ed.* **2007**, *46* (24), 4477−4480.
(27) Sousa, F. L.; Bogge, H.; Merca, A.; Gouzerh, P.; Thouvenot, R.; Müller, A. *Chem. Commun.* **2009**, *48*, 7491−7493.
(28) Keita, B.; Kortz, U.; Holzle, L. R. B.; Brown, S.; Nadjo, L. *Langmuir* **2007**, *23* (19), 9531−9534.
(29) Hijazi, A.; Kemmegne-Mbouguen, J. C.; Floquet, S.; Marrot, J.; Mayer, C. R.; Artero, V.; Cadot, E. *Inorg. Chem.* **2011**, *50*, 9031−9038.
(30) Duval, S.; Floquet, S.; Simonnet-Jégat, C.; Marrot, J.; Biboum, R. N.; Keita, B.; Nadjo, L.; Haouas, M.; Taulelle, F.; Cadot, E. *J. Am. Chem. Soc.* **2010**, *132* (6), 2069−2077.
(31) Keita, B.; Floquet, S.; Lemonnier, J. F.; Cadot, E.; Kachmar, A.; Bénard, M.; Rohmer, M. M.; Nadjo, L. *J. Phys. Chem. C* **2008**, *112* (4), 1109−1114.
(32) Béreau, V.; Cadot, E.; Bogge, H.; Müller, A.; Sécheresse, F. *Inorg. Chem.* **1999**, *38* (25), 5803−5808.
(33) Pilette, M.-A.; Marrot, J.; Sécheresse, F.; Cadot, E. *Inorg. Chim. Acta* **2010**, *363*, 4253−4261.
(34) Cadot, E.; Béreau, V.; Marg, B.; Halut, S.; Sécheresse, F. *Inorg. Chem.* **1996**, *35* (11), 3099−3106.
(35) Cadot, E.; Béreau, V.; Sécheresse, F. *Inorg. Chim. Acta* **1996**, *252* (1−2), 101−106.
(36) Marrot, J.; Pilette, M. A.; Sécheresse, F.; Cadot, E. *Inorg. Chem.* **2003**, *42* (11), 3609−3615.
(37) Cadot, E.; Pilette, M. A.; Marrot, M.; Sécheresse, F. *Angew. Chem., Int. Ed.* **2003**, *42* (19), 2173−2176.
(38) Pilette, M.-A.; Floquet, S.; Marrot, J.; Cadot, E. *Eur. J. Inorg. Chem.* **2011**, 3523−3528.
(39) Keita, B.; Nadjo, L. *J. Electroanal. Chem.* **1988**, *243* (1), 87−103.
(40) Cadot, E.; Salignac, B.; Marrot, J.; Dolbecq, A.; Sécheresse, F. *Chem. Commun.* **2000**, *4*, 261−262.
(41) Lemonnier, J. F.; Floquet, S.; Marrot, J.; Cadot, E. *J. Cluster Sci.* **2006**, *17* (2), 267−282.
(42) Lemonnier, J. F.; Duval, S.; Floquet, S.; Cadot, E. *Isr. J. Chem.* **2011**, *51* (2), 290−302.
(43) Modec, B.; Brencic, J. V.; Zubieta, J. *J. Chem. Soc., Dalton Trans.* **2002**, 1500−1507.
(44) Keita, B.; Lu, Y. W.; Nadjo, L.; Contant, R. *Electrochem. Commun.* **2000**, *2* (10), 720−726.